Chapter 5: Probing the Role of the Peptide Backbone in the Aromatic Binding Box of the nAChR

5.1 Introduction

The residues that are involved in agonist-binding in the nicotinic acetylcholine receptor (nAChR) have been known for over two decades.[1] Even before any structural data were available, researchers had identified several key aromatic residues important to agonist binding. These amino acids include αY93, αW149, αY190, αY198, and γW55 and δW57. The AChBP crystal structure confirmed the importance of these residues and indicated they form a box like configuration around the agonist.[2] This "aromatic binding box" is shown in Figure 5.1. The recent crystal structures of AChBP with and without agonist bound and decades of careful biochemical studies have yielded a substantial amount of information about the interactions between nAChR and agonist.

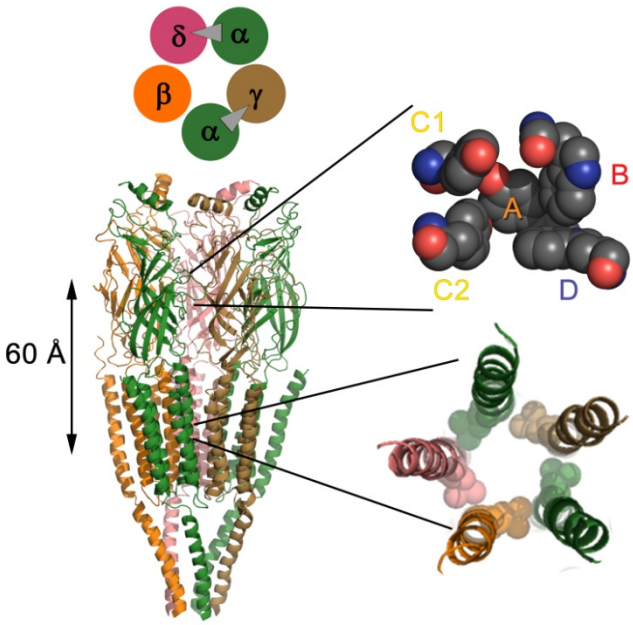

Figure 5.1: Overall structure of the muscle nAChR. The location of the aromatic binding box (upper right) and the putative channel gate (lower right) are indicated.

Considerably less is known about how the conformational changes that accompany binding interface with channel gating. Single channel electrophysiology of the nAChR coupled

with linear free energy analysis has inspired the idea that a "conformational wave," a series of progressive conformational changes originating at the binding site and terminating at the channel gate, is responsible for coupling agonist binding to channel opening.[3, 4] Linear free energy analysis indicates that blocks of residues encompassing the agonist binding site move early in the gating transition, that is, the motions that initiate the conformational wave originate in the vicinity of aromatic binding box. In further support of this idea, the side chains of three residues near the acetylcholine binding site, αY190, αD200, and αK145, have been shown to influence gating and are proposed to initiate the allosteric cascade that links binding to gating.[5] In addition to the importance of specific side chains present near the binding site, significant movement along the protein backbone is probably necessary to propagate the conformational changes that result in channel gating.

To interrogate the role of the peptide backbone in the agonist binding site in initiating the gating cascade, ten individual ester mutations were made to the backbone of the aromatic box residues and their i+1 neighbors. Combined, these mutations disrupted the hydrogen bonding ability at all non-carbon backbone positions of the aromatic box residues; the ester mutation at the box residue directly eliminates a hydrogen bond donor and the ester mutation at the i+1 residue decreases the hydrogen bonding ability of the adjacent carbonyl (of the box residue). In addition, the incorporation of a backbone ester endows a greater amount of backbone flexibility by removing the pronounced amide resonance. The conjugation of the H-N-C=O moiety in amides leads to a significantly higher barrier to interconversion between the trans and cis isomers, although the trans preferences in esters is stronger than in amides for steric reasons. Thus, if backbone motions in the aromatic binding box are important for

initiating the conformational changes that transduce agonist binding into channel opening, ester incorporation at these sites will significantly impact receptor function.

5.2 Results and Discussion

5.2.1 α-Hydroxy Incorporation at Aromatic Box Residues in the Primary Subunit.

Ester mutations were made at the aromatic box residues, αY93, αW149, αY190, αY198, and their i +1 neighbors, αN94, αT150, αS191, αL199, in the primary binding subunit. One ester mutation, at αS191, led to a severe loss of function and an impairment of channel gating. The backbone NH at this residue was found to make an important intersubunit hydrogen bond and is discussed in detail in Chapter 2. However, the majority of the α-hydroxy mutations at these sites produced very little effect on receptor function (less than 2-fold change in EC_{50}, Figure 5.2 and Table 5.1). Two sites, αT150 and αL199, had intermediate effects on receptor function, producing approximately 5-fold shifts in EC_{50} values. An ELFCAR analysis[6] (see Chapter 4) revealed that, with the exception of the αS191Sah mutation, the loss-of-function mutants had normal Ω-values, indicating that ester incorporation does not severely impair the gating behavior of these receptors.

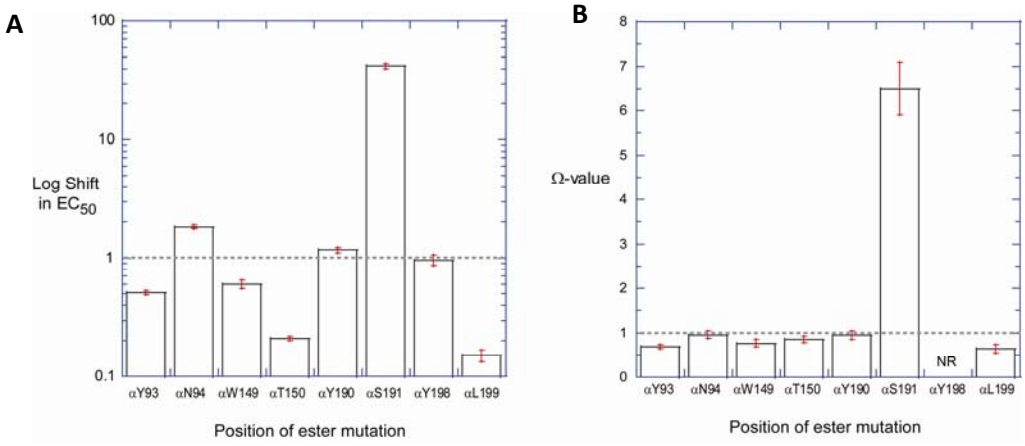

Figure 5.2: A) The log fold shifts in EC_{50} values for α-hydroxy mutations in the α-subunit. B) The corresponding Ω-values for these mutations.

Table 5.1: Fold shifts in EC_{50} values and Ω-values for backbone ester mutations in the α-subunit

Position of ester mutation	EC_{50} Shift	Ω-value
αY93	0.51 ± 0.02	0.69 ± 0.05
αN94	1.8 ± 0.07	0.96 ± 0.08
αW149	0.60 ± 0.05	0.77 ± 0.08
αT150	0.21 ± 0.009	0.86 ± 0.08
αY190	1.2 ± 0.07	0.95 ± 0.09
αS191	42 ± 2	6.5 ± 0.6
αY198	0.96 ± 0.1	NR
αL199	0.15 ± 0.02	0.64 ± 0.09

The αT50Tah mutation has been studied previously.[7, 8] Originally the backbone NH of this residue combined with the backbone NH of neighboring αW149 was proposed to interact with a critical aspartate residue (αD89) to promote an efficient interaction between αW149 and agonist.[9] However, experimental work does not corroborate this hypothesis. Instead, αT150 and αW149 backbone amides seem to belong to a network of redundant hydrogen bonds in this region that hold the side chain of αW149 in place for agonist binding.[8]

An approximately five fold decrease in EC_{50} was observed for the α-hydroxy mutant of αL199, indicating a moderate gain-of-function. None of the existing structures (Torpedo cryo-EM,[10] AChBP crystal structures,[11] or the α_1 mm nAChR crystal structure[12]) show any hydrogen bonds to the backbone NH of αL199. A further analysis of the hydrogen bonds to the protein backbone at αL199 in a 7 ns MD simulation of a homology model of the muscle nAChR extracellular domain (see Chapter 6) further shows very little hydrogen bonding to the NH throughout the trajectory (Figure 5.3A).

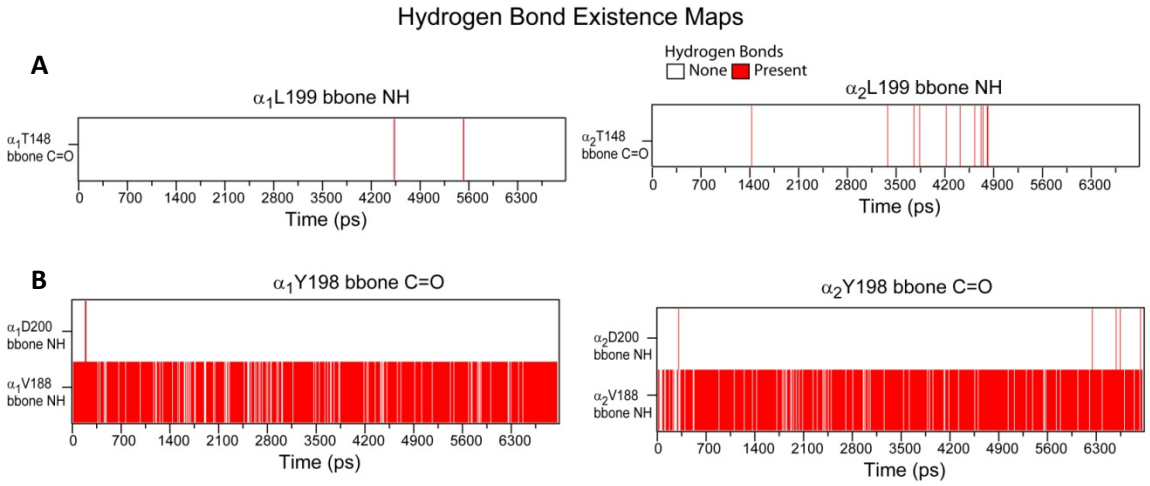

Figure 5.3: Hydrogen bond analysis of the moieties affected by the backbone ester mutation at αL199in the αγ (left) and αδ (right) binding sites. A) Hydrogen bonds formed with the αL199 NH. B) Hydrogen bonds formed with the αY198 cabonyl.

Replacing the backbone NH with an oxygen diminishes the hydrogen bonding ability of the neighboring carbonyl, in this case, the C=O group on αY198. Examining the hydrogen bonding pattern of this moiety reveals a hydrogen bond to the backbone NH of αV188 that is present throughout the 7 ns simulation (Figure 5.3B). This hydrogen bond is between the two β-sheets flanking the C-loop and may provide some structural rigidity to this region of the protein. Therefore, the weakening of this hydrogen bond, combined with increased backbone flexibility at αL199, may result in greater C-loop mobility. Numerous studies implicate the closure of the C-loop upon agonist binding in early transduction of the signal from agonist binding to channel pore opening.[6, 13, 14] A plausible model posits that the inward motion of the C-loop pulls at the flanking β-sheets (β7β10), changing crucial interactions between the interfacial residues of the extracellular and transmembrane domains. The putative increased ability of the C-loop to undergo this inward motion as a result of the increased backbone flexibility endowed by the αL199Lah mutation would thus make the receptor easier to open, leading to the observed gain-of-function behavior. As this mutation leads to a decrease in the EC_{50} value, the ELFCAR

analysis[6] is unable to detect whether a significant change in gating underlies the macroscopic phenotype.

5.2.2 Biphasic Behavior of Complementary Binding Site Ester Mutations

5.2.2.1 Whole-Cell Electrophysiological Characterization of the Biphasic Phenotype

Mutating the aromatic box residue contributed by the complementary binding subunit, γW55/δW57, to its analogous α-hydroxy acid leads to anomalous receptor behavior. Simultaneous ester incorporation at these sites alone leads to an unremarkable ~2-fold shift in EC_{50} (Figure 5.4A). However, in the presence of the L9'S pore mutation in any subunit, a two-component (biphasic) dose-response relation was observed (Figure 4B). Moreover, the macroscopic behavior was dramatically different when the binding sites were mutated individually. Mutating the δ-subunit alone (in conjunction with the βL9'S pore mutation) gave a monophasic dose-response curve with an EC_{50} value that is consistent with the typical 40-fold decrease observed with the βL9'S mutation. An ester mutation at this position in the γ-subunit, however, exhibited biphasic behavior, similar to that observed for the double binding site mutant receptor (Figure 5.4C).

One potential explanation for this behavior is that the ester mutation in the non-α aromatic binding box residue prevents proper subunit assembly. For example, if the γW55Wah subunit is inefficiently expressed or incorporated into the pentameric receptor, the δW57Wah subunit could act as a replacement. This would lead to both α_2β9'γ55Wah δ57Wah and α_2 β9'$(\delta 57Wah)_2$ receptors, with this mixed population giving rise to the observed biphasic behavior. Poor incorporation efficiency has been demonstrated to produce multicomponent

dose-response relations[15] and both γ-less and δ-less mouse muscle nAChRs have been observed.[16, 17]

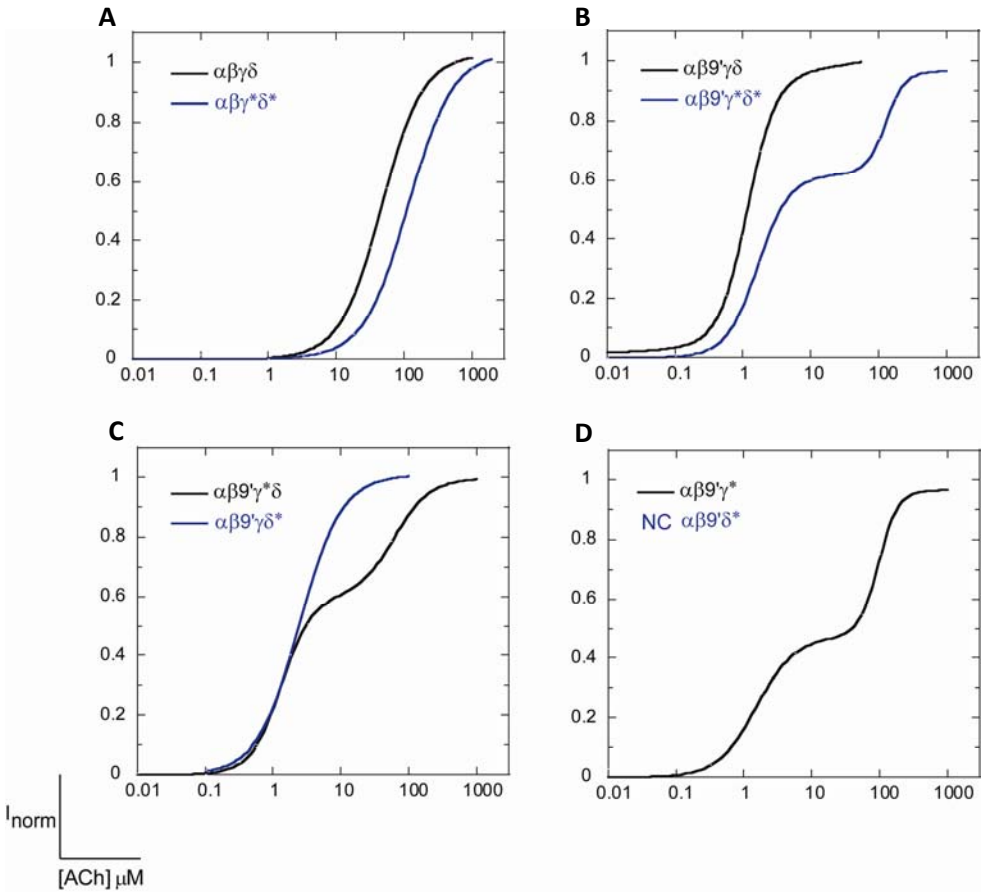

Figure 5.4: Dose-response relations of the wild-type and backbone ester mutations at γW55/δW57. A) No L9'S pore mutation. WT is in black, ester mutant is in blue. B) βL9'S pore mutation. WT is in black. Ester mutant is in blue. C) Differential effects of ester incorporation in only one subunit. γ-only is in black, δ-only is in blue. D) Subunit omission. The black curve is the δ-less receptor with the ester mutation in γ and the βL9'S pore mutation. No currents were observed for the ester-containing γ-less receptors.

Subunit-less experiments, in which the mRNA for either the γ or the δ-subunits was omitted, were performed to examine the issue of subunit incorporation. The γ-less receptors did not express, while the δ-less receptors produced biphasic dose-response behavior (Figure 5.4D). While the ability of δ-less receptors to express supports the inefficient incorporation hypothesis, the fact that these receptors themselves produce biphasic dose-response relations does not. No obvious stochiometic mixture for two δ-less receptors could retain two functional

binding sites, as the mouse muscle β-subunit is not known to function as a binding subunit. These data thus beg the question: can the observed biphasic behavior arise from a homogeneous receptor population?

5.2.2.2 Biphasic Behavior is Theoretically Possible From a Single Receptor Population

Cys-loop ligand-gated ion channels function by allosteric transitions between various closed (non-conducting) and open (ion conducting) states.[4, 18, 19] In principle, these transitions may occur with or without the binding of agonist, although spontaneous (agonist-free) openings occur with very low probability. In the case of the muscle nAChR, the binding of two molecules of agonist are required for efficient channel opening (Figure 5.5). Once agonist binds to the receptor, it induces conformational changes of the receptor from a resting state (closed channel) to an activated state (open channel). Activation may be followed by the return to the resting state following agonist dissociation or by a transition to an agonist-bound desensitized state (closed channel). Because the diliganded open state is strongly energetically preferred over the diliganded closed state, the open state of the receptor has a much higher affinity for agonists than the closed state of the receptor (nanomolar versus micromolar). This ensures two things; first, that once two molecules of agonist bind, the receptor opens quickly, and second, that if the receptor opens with only one molecule of agonist bound (monoliganded opening), the second molecule of agonist rapidly binds to produce the energetically favorable diliganded open state.

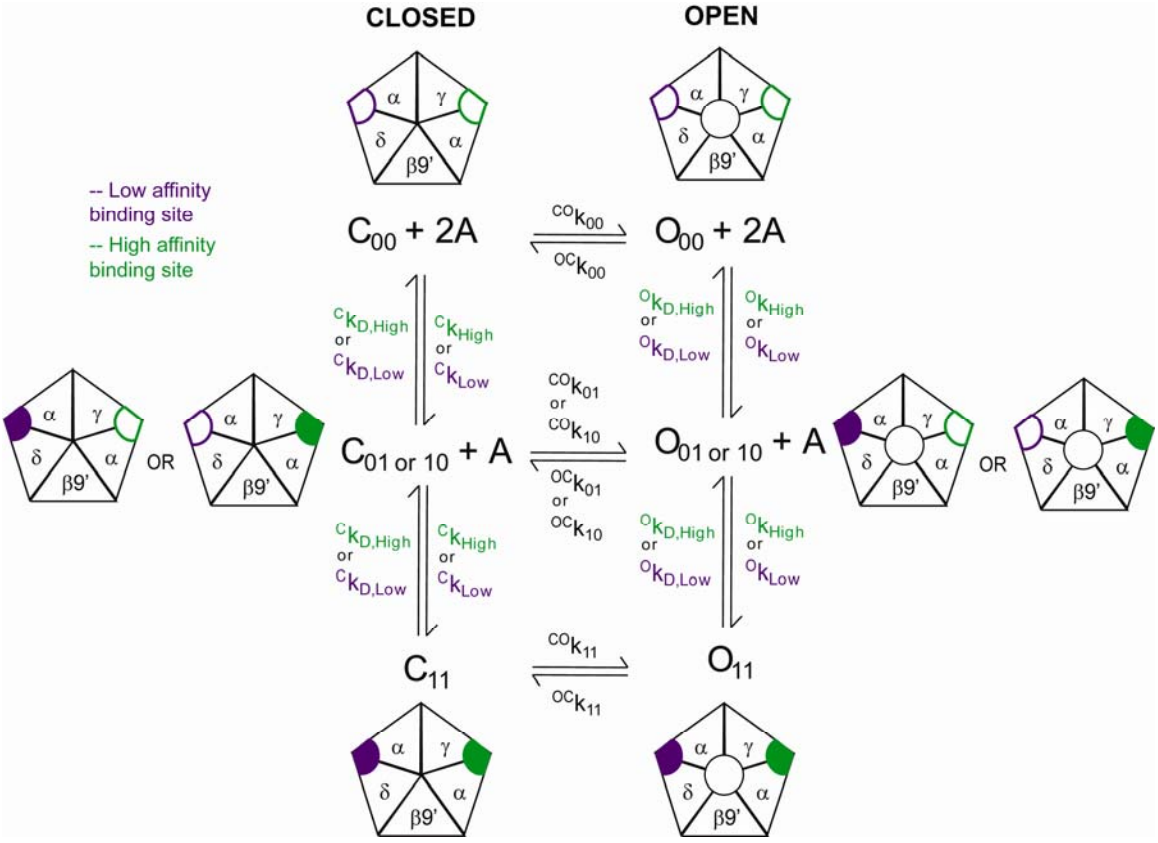

Figure 5.5: Basic kinetic scheme for the muscle nAChR. Moving from left to right represents a channel opening event. Moving from top to bottom represents a ligand-binding event. Purple and green are used to denote the nonequivalent low and high affinity acetylcholine binding sites, resprectively.

The kinetics of these allosteric transitions are governed by rate constants related to the energy barriers between allosteric states. These parameters determine the probability with which any individual ion channel will be found in a given conformation at any instant in time. These rate constants include (1) on and off rate constants for agonist binding, (2) rates constants for the transition from the resting to activated state, and (3) rate constants for transitions out of the activated state to the desensitized or resting states. A full complement of rate constants permits a complete description of the system and allows for the prediction of ion channel behavior both on the single channel and macroscopic levels.

In order to determine if biphasic dose-response behavior can arise simply by varying the rate constants in the standard kinetic model of the muscle nAChR, we employed the program STOIC (Simulations of Transient Openings of Ionotropic-receptor Channels).[20] This program employs a kinetic-based Monod-Wyman-Changeux allosteric model based on linear free energy relations to describe the effects of ligand binding events on interconversions between closed, open, and desensitized conformations of a single channel. Ensemble averages of these single channel simulations can be used to generate macroscopic dose-response data and thus EC_{50} values. The kinetic scheme for STOIC allows the user to control the on and off rates for agonist binding, as well as interconversion rates among resting, activated, and desensitized states. STOIC also allows for non-equivalent binding sites, which is crucial in modeling a receptor that displays differential behavior at each binding site.

Before using STOIC to simulate the mutant dose-response behavior, wild-type behavior was modeled using reported rates from experimental single-channel studies, where available (Table 5.2). These rates provided a starting point for lengthy, but non-exhaustive, efforts to determine the rates constants responsible for inducing a change from a monophasic to biphasic dose-response curve. The successful generation of a two-component dose-response relation based on adjusting the kinetic parameters within the standard model for receptor action means that the observed biphasic behavior of the γ55Wahδ57Wah receptors could be produced by a single receptor population.

A number of biphasic dose-response curves were produced with a variety of combinations of kinetic parameters. However, there was a consistent trend in the equilibrium dissociation constants when comparing the monophasic and biphasic curves: the affinity of the low affinity binding site for agonist in the open state is *less* than the affinity of the high affinity

binding site for agonist in the closed state (Table 5.2). Stated otherwise, the monoliganded open state (low affinity site occupied) has become an energetically favorable state, leading to monoliganded openings making a significant contribution to the overall open state of the receptor. This suggests monoliganded openings as a possible origin for biphasic dose-response behavior arising from a single, homogenous receptor population.

		monophasic	monophasic	**biphasic**	**biphasic**	monophasic	monophasic
		WT	**αβ9'γδ**				
(s^{-1})	$^{c}k_{High}$	1.00E+08	1.00E+08	1.00E+08	1.00E+08	1.00E+08	1.00E+08
	$^{c}k_{D,High}$	5200	235	50	553.15	10000	553.15
	$^{c}k_{Low}$	1.00E+08	1.00E+08	1.00E+08	1.00E+08	1.00E+08	1.00E+08
	$^{c}k_{D,Low}$	1.04E+05	1175.00	8.00E+05	8.00E+05	8.00E+05	8.00E+05
($M^{-1}s^{-1}$)	$^{o}k_{High}$	1.00E+08	1.00E+08	1.00E+08	1.00E+08	1.00E+08	1.00E+08
	$^{o}k_{D,High}$	1.6	0.35	1.2381	1.2381	1.2381	1.2381
	$^{o}k_{Low}$	1.00E+08	1.00E+08	1.00E+08	1.00E+08	1.00E+08	1.00E+08
	$^{o}k_{D,Low}$	32	1.75	6500	30000	6500	100
	$^{c}Kd_{eq,High}$	5.20E-05	2.35E-06	5.00E -07	5.53E -06	1.00E-04	5.53E-06
	$^{c}Kd_{eq,Low}$	1.04E-03	1.175E-05	8.00E-03	8.00E-03	8.00E-03	8.00E-03
	fold affinity	20	5	**16000**	**1446**	**80**	**1446**
	$^{o}Kd_{eq,High}$	1.60E-08	3.50E-09	1.24E-08	1.24E-08	1.24E-08	1.24E-08
	$^{o}Kd_{eq,Low}$	3.20E-07	1.75E-08	6.50E -05	3.00E -04	6.50E-05	1.00E-06
	fold affinity	20	5	**5250**	**24231**	**5250**	**81**

Table 5.2: Parameters used in STOIC simulations.

5.2.2.3 Anomalous receptors display normal receptor stochiometry

To experimentally probe for correct subunit assembly, single molecule photobleaching experiments were undertaken. For these experiments, EGFP was inserted into the M3-M4 linker of the β- and γ-subunits. These EGFP-containing proteins were then further fluorescently

labeled using the competitive antagonist α-bungarotoxin monoconjugated to the Alex488 fluorophore.

Photobleaching of a single fluorescent molecule is a discrete process. A stepwise decrease in fluorescence intensity results for a protein-ligand complex containing several fluorescent molecules, with the number of observed photobleaching steps corresponding to the number of fluorescent moieties in the complex. In principle, the number of photobleaching steps would exactly equal the number of fluorescent molecules. In reality, however, a distribution of photobleaching steps is observed. This distribution reflects a number of contributing phenomena. First, due to the experimental set up, a subset of fluorescent molecules will photobleach prior to image acquisition. Second, a significant percentage (~20%) of "fluorescent" proteins are nonfluorescent. Thirdly, incomplete labeling of the receptors with α-bungarotoxin and/or imperfectly labeled αBtxA488 reagent reduces the number of observed photobleaching steps. Finally, more than the anticipated number of photobleaching steps is occasionally observed due to either the colocalization of two receptors or an αBtx labeled with more than one Alexa488 molecule. Therefore, in addition to counting the number and distribution of photobleaching steps, comparing the distribution of photobleaching steps between the wild-type and mutant proteins is necessary to assess differences in receptor subunit composition.

To confirm normal receptor assembly, three sets of experiments were performed. In the first, the β-subunit was tagged with EGFP, and the receptor was labeled with αBtxA488. Both WT and mutant receptors bearing an EGFP containing β-subunit and labeled with αBtxAlexa488 displayed puncta with 1 (29%, 25%, respectively), 2 (46%, 38%), 3 (24%, 28%), and 4-6 (7%, 9%) photobleaching steps (Figure 5.6A). This confirmed the incorporation of the β-

subunit into the mutant receptors, however, it could not distinguish whether the mutant receptors contained two different binding sites (e.g., one αγ and one αδ) or two αδ or two αγ. Therefore, a subsequent experiment was needed to confirm that we were not observing γ-less or δ-less receptors.

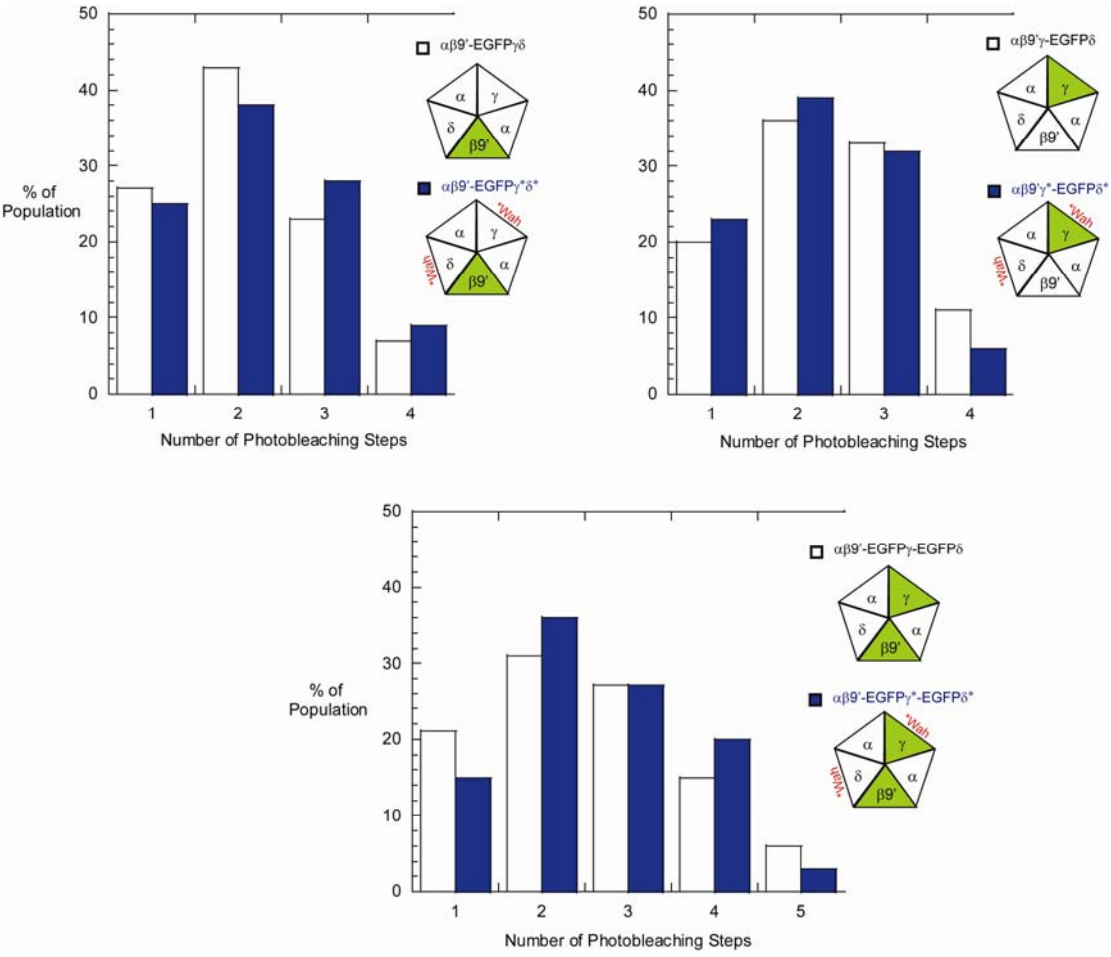

Figure 5.6: Photobleaching histograms. White and blue bars represent the wild-type and double ester-containing receptors, respectively. In all cases, receptors were labeled with αBtxA488. A) β9'-EGFP B) γ-EGFP C) β9'-EGFP and γ-EGFP.

An EGFP-tagged γ-subunit labeled with αBtxAlexa488 is used to probe whether the γ-subunit is normally assembled into the receptor. Three photobleaching steps would indicate that the fluorescently labeled γ-subunit is assembled correctly in the receptor. Alternatively, four photobleaching steps would be seen if there are two αγ binding sites and only two

photobleaching steps would be observed if there are two αδ binding sites. By comparing the photobleaching profiles of the αβ9'γ55Wahδ57Wah mutants with that of wild type receptors, it was possible to determine that these receptors were assembled normally. Both wild type and mutant receptors bearing an EGFP containing γ-subunit and labeled with αBtxAlexa488 displayed puncta with 1 (13%, 26%, respectively), 2 (23%, 44%), 3 (21%, 36%), and 4-6 (7%, 7%) photobleaching steps (Figure 5.6B).

An additional experiment was done wherein EGFP-bearing β and γ subunits were expressed and subsequently labeled with αBtxAlexa488. WT-like photobleaching profiles with a maximum of four photobleaching steps were observed, confirming correct receptor assembly. In this case, the photobleaching profiles were as follows: 21%, 15% displayed one photobleaching step, 31%, 36% showed two photobleaching steps, 27%, 27% displayed three photobleaching steps, 15%, 20% had four photobleaching steps, and 6%,3% had five or more photobleaching steps for WT and mutant receptors, respectively (Figure 5.6C).

Overall, the distribution of photobleaching steps of the mutant receptors is consistent with that of the WT receptors, confirming a stochiometric subunit population similar to that of the wild-type receptors. These data do not rule out heterogeneity in the receptor population, but do strongly suggest a receptor population that is homogeneous with respect to subunit composition.

5.2.2.4 Biphasic behavior: novel phenomenon or experimental artifact?

Typically a biphasic dose-response curve is indicative of a mixed population of receptors. Through kinetic modeling it was shown that this behavior can theoretically be produced by a single population of receptors. However, an alternative possibility is that one of the

components is the result of re-aminoacylation of the suppressor tRNA (see also Chapter 1). Based on the original data set collected, several lines of evidence would suggest against this.

Two types of control experiments are used to detect re-aminoacylation, as described in Chapter 1. The first involves co-injecting uncharged suppressor tRNA along with the mRNA containing the stop codon at the site(s) of interest. This control typically yielded no detectable currents and in no case gave current sizes above 10% of the experimental response, where Wah-tRNA or Trp-tRNA was co-injected. On a single day, currents from the re-aminoacylation control produced currents from which a reliable dose-response relation could be constructed, giving an EC_{50} value of 480 μM. The average current size of such control experiments was approximately 160 nA, while the experimental data displayed currents in the tens of microamperes range. The second control involves the recovery of the wild-type phenotype by co-injecting the natural amino acid appended to the suppressor tRNA with the mutant mRNA. Robust currents of a similar size of the Wah-tRNA experimental work were observed, but no biphasic behavior was observed. Robust current sizes and monophasic dose-response relations were also observed for the incorporation of both Tyr and Yah at γW55 and δW57. If one of the components of the biphasic dose-response were a result of re-aminoacylation, then this component should have also been present in other suppression experiments.

In addition to the control experiments, two other experimental results strongly suggest that re-aminoacylation did not lead to the originally observed two-component dose response. First, the dose-response relations for partial agonists epibatidine and succinylcholine for the αβ9γW55WahδW57Wah receptors are monophasic (Figure 5.7). Importantly, the monophasic behavior of these partial agonists was observed on the same day as biphasic behavior was observed for acetylcholine. Second, the differential behavior of the two binding sites provides

some support for the idea that the biphasic phenomenon is not a result of re-aminoacylation. However, differential incorporation of the re-aminoacylated amino acid at the two binding sites might also explain this behavior.

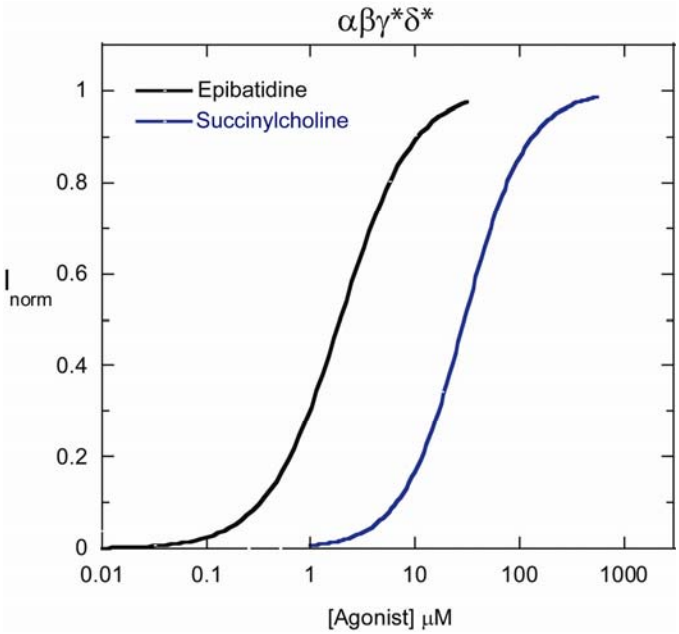

Figure 5.7: Dose-response curves of αβ9'γ55Wahδ57Wah receptors for partial agonists epibatidine and succinylcholine.

The experiments listed above were conducted between the spring of 2006 and the spring of 2008. Upon encountering expression problems in the summer of 2008, the mutant mRNA was re-made and tryptophan α-hydroxy was re-synthesized, at which point it was discovered that the original stock had been racemic. Both racemic and S-Wah were synthesized and shown to produce similar shifts in EC_{50}. However, at this point the biphasic dose-response behavior was no longer observed. In addition, significant current from the 76mer control was observed. Although the appearance of 76mer current did not correspond to the observation of biphasic dose-response behavior, it did raise concerns that the original biphasic data was a result of a mixed receptor population. Without being able to reproduce the biphasic behavior, it is impossible to draw any conclusions from the original data det.

5.3 Materials and Methods

5.3.1 Whole-cell Electrophysiology and data analysis

Electrophysiological measurements were carried out 18-72 hours post-microinjection. Macroscopic measurements were performed with a two-electrode voltage-clamp circuit using an OpusXpress (Axon Instruments, Foster City, CA). Oocytes were bathed in the extracellular recording solution Ca^{2+} -free ND96 (96 mM NaCl, 2 mM KCl, 1 mM $MgCl_2$ ($6H_2O$, 5 mM HEPES, pH 7.4). ACh-induced currents were recorded in response to bath application of acetylcholine (flow rate of 4 mL/min for 15 seconds) at a holding potential of -60 mV. Data were sampled at 125 Hz and filtered at 50 Hz. Individual dose-response data were fit to the Hill equation (Equation 1) where I is the current, Imax is maximal current, [A] is agonist concentration, EC_{50} is the concentration to elicit a half-maximal response, and n is the Hill coefficient.

$$y = I_{\max} * \frac{[A]^n}{[A]^n + EC_{50}^n} \tag{5.1}$$

Biphasic dose-response data were fit with a two component Hill equation (Equation 2) where c1 is the weighted value corresponding to the lower EC_{50} component.

$$y = I_{\max} * \left[c_1 * \frac{[A]^{n1}}{[A]^{n1} + EC_{50,1}^{n1}} + (1 - c_1) * \frac{[A]^{n2}}{[A]^{n2} + EC_{50,2}^{n2}} \right] \tag{5.2}$$

Macroscopic data represent measurements obtained from 5-27 individual oocytes.

5.3.2 STOIC

The STOIC simulation program is designed to run in the MATLAB environment. STOIC is available upon request via the internet at

<http://www.unige.ch/sciences/biochemie/Edelstein/research.html>. The parameters used in this model are given in the Results and Discussion section.

5.3.3 Single-molecule labeling and TIRF microscopy

GFP-tagged subunits were created using an integration of PCR fragments technique, which does not require the use of restriction enzymes. Forward and reverse primers for pEGFP-N1 vector (Clontech; excitation maximum = 488 nm; emission maximum = 507 nm) were designed with 5' overhangs of 24 nucleotides corresponding to the eight amino acid residues immediately before and after the desired insertion site of the nAChR subunit (after position P350 in β and L351 in γ). A GFP fragment with overhangs was amplified by 30 cycles of PCR and purified by extraction from a 1% agarose gel using a QIAquick gel extraction kit (Qiagen). Concentration of purified GFP fragment with overhangs was quantified using a NanoDrop spectrophotometer (NanoDrop Technologies). The GFP fragment was then inserted into the appropriate nAChR subunit vector with a 5:1 mass ratio of insert:destination vector by 18 cycles of PCR. GFP-tagged nAChR subunit DNA was obtained by DpnI digest and transformed using Blue Top10 cells by electroporation. Colonies were picked and the complete EGFP inserted nAChR subunit DNA was identified by DNA sequencing.

Xenopus oocytes were prepared for imaging by TIRF microscopy by first stripping the vitalline membrane with forceps, following immersion in a hypertonic solution (220 mM NaAspartate, 10 mM HEPES, 10 mM EDTA, 2 mM MgCl2, pH 7.38) for five to ten minutes. The oocytes were subsequently placed, animal pole down, on a clean glass coverslip in an imaging chamber on the microscope stage. The room was cooled to 15- 20 C to both minimize drift and maintain the health and mechanical stability of the oocytes. The TIRF microscope was a Melles-Griot Argon (Ar) ion laser connected via a fiber optic to an Olympus TIRF illuminator adapted to

a standard inverted IX-71 Olympus microscope (Center Valley, PA). An excitation wavelength of 488 nm was selected to excite and detect the Alexa488 and eGFP fluorophores using a Z488 filter cube from Chroma Technology Corporation (Rockingham, VT). Time-lapse images were captured over a period of 5- 20 minutes using a Photometrics Cascade front illuminated CCD camera from Princeton Instruments (Trenton, NJ). Data were acquired on Slidebook from Intelligent Imaging Innovations Inc (Santa Monica, CA) and then analyzed using ImageJ (National Institutes of Health), Clampfit 9.2 (Axon Instruments, Foster City, CA), and Origin 7.0 (OriginLab, Northhampton, MA).

Analysis was performed by examining the fluorescence profiles of puncta imaged over several minutes. Puncta that did not result in discrete photobleaching steps during the acquisition were excluded from analysis. In addition, the analysis was limited to cases where fewer than 0.3 puncta/μm^2 were observed in order to avoid excess co-localization of receptors within a diffraction-limited spot.

5.4 References

1. Changeux, J.P. & Edelstein, S.J. Nicotinic Acetylcholine Receptors: From Molecular Biology to Cognition (Odile Jacob, New York, 2005).
2. Brejc, K. et al. Crystal structure of an ACh-binding protein reveals the ligand-binding domain of nicotinic receptors. *Nature* **411**, 269-76 (2001).
3. Auerbach, A. Life at the top: the transition state of AChR gating. *Sci STKE* **2003**, re11 (2003).
4. Colquhoun, D. From shut to open: what can we learn from linear free energy relationships? *Biophys J* **89**, 3673-5 (2005).
5. Sine, S.M. & Engel, A.G. Recent advances in Cys-loop receptor structure and function. *Nature* **440**, 448-55 (2006).
6. Gleitsman, K.R., Lester, H.A. & Dougherty, D.A. Probing the role of backbone hydrogen bonding in a critical beta sheet of the extracellular domain of a cys-loop receptor. *Chembiochem* **10**, 1385-91 (2009).
7. Cashin, A.L., Petersson, E.J., Lester, H.A. & Dougherty, D.A. Using physical chemistry to differentiate nicotinic from cholinergic agonists at the nicotinic acetylcholine receptor. *J Am Chem Soc* **127**, 350-6 (2005).
8. Cashin, A.L., Torrice, M.M., McMenimen, K.A., Lester, H.A. & Dougherty, D.A. Chemical-scale studies on the role of a conserved aspartate in preorganizing the agonist binding site of the nicotinic acetylcholine receptor. *Biochemistry* **46**, 630-9 (2007).
9. Lee, W.Y. & Sine, S.M. Invariant aspartic Acid in muscle nicotinic receptor contributes selectively to the kinetics of agonist binding. *J Gen Physiol* **124**, 555-67 (2004).
10. Unwin, N. Refined structure of the nicotinic acetylcholine receptor at 4A resolution. *J Mol Biol* **346**, 967-89 (2005).
11. Rucktooa, P., Smit, A.B. & Sixma, T.K. Insight in nAChR subtype selectivity from AChBP crystal structures. *Biochem Pharmacol* **78**, 777-87 (2009).
12. Dellisanti, C.D., Yao, Y., Stroud, J.C., Wang, Z.Z. & Chen, L. Crystal structure of the extracellular domain of nAChR alpha1 bound to alpha-bungarotoxin at 1.94 A resolution. *Nat Neurosci* **10**, 953-62 (2007).
13. Law, R.J., Henchman, R.H. & McCammon, J.A. A gating mechanism proposed from a simulation of a human alpha7 nicotinic acetylcholine receptor. *Proc Natl Acad Sci U S A* **102**, 6813-8 (2005).
14. McLaughlin, J.T., Fu, J., Sproul, A.D. & Rosenberg, R.L. Role of the outer beta-sheet in divalent cation modulation of alpha7 nicotinic receptors. *Mol Pharmacol* **70**, 16-22 (2006).
15. Covernton, P.J. & Connolly, J.G. Multiple components in the agonist concentration-response relationships of neuronal nicotinic acetylcholine receptors. *J Neurosci Methods* **96**, 63-70 (2000).
16. Charnet, P., Labarca, C. & Lester, H.A. Structure of the gamma-less nicotinic acetylcholine receptor: learning from omission. *Mol Pharmacol* **41**, 708-17 (1992).
17. Francis, M.M. & Papke, R.L. Muscle-type nicotinic acetylcholine receptor delta subunit determines sensitivity to noncompetitive inhibitors, while gamma subunit regulates divalent permeability. *Neuropharmacology* **35**, 1547-56 (1996).

18. Colquhoun, D. Binding, gating, affinity and efficacy: the interpretation of structure-activity relationships for agonists and of the effects of mutating receptors. *Br J Pharmacol* **125**, 924-47 (1998).
19. Jackson, M.B. Perfection of a synaptic receptor: kinetics and energetics of the acetylcholine receptor. *Proc Natl Acad Sci U S A* **86**, 2199-203 (1989).
20. Edelstein, S.J., Schaad, O., Henry, E., Bertrand, D. & Changeux, J.P. A kinetic mechanism for nicotinic acetylcholine receptors based on multiple allosteric transitions. *Biol Cybern* **75**, 361-79 (1996).